continuous bridges. The SMA reinforcing bars are implemented in the fixed piers of bridges to generate self-centering responses while the required energy dissipation is provided by using friction dampers at movable substructures like abutments. Design method is developed for balanced seismic performance between SMAs and friction on the system level. Using static pushover and dynamic time-history analyses, different longitudinal bridge systems are evaluated and compared, including the proposed self-centering system with balanced SMAs and friction. The outcome of the current study is expected to provide an alternative method for improving the energy dissipation of the SMA-based self-centering bridges. The study can also provide a more thorough understanding of the balanced seismic design concept between energy dissipation and self-centering capacities.

2. PROTOTYPE AND STRENGTHENED BRIDGES AND MODELLING

The selected prototype bridge in this study is a two-span continuous reinforced concrete (RC) bridge with one fixed pier and two movable abutments, or more specifically, fixed bearings are placed at the pier while expansion movable bearings are installed at the abutments. The span length of the bridge is 25 m with T-shaped RC girders adopted as the superstructure. The unit weight of the superstructure is estimated as 22.7 ton/m, assuming uniformly distributed along the span length. The fixed pier is a double-column RC bent structure, having the effective height of 8 m and the column diameter of 1.6 m. The concrete used for the pier construction has a design compressive strength of 26.8 MPa, whereas the design tensile yield strength for the steel reinforcement is 400 MPa. The initial gap between the superstructure girders and the abutment backwalls is 0.08 m. Group pile foundations are adopted at the base of the pier and abutments.

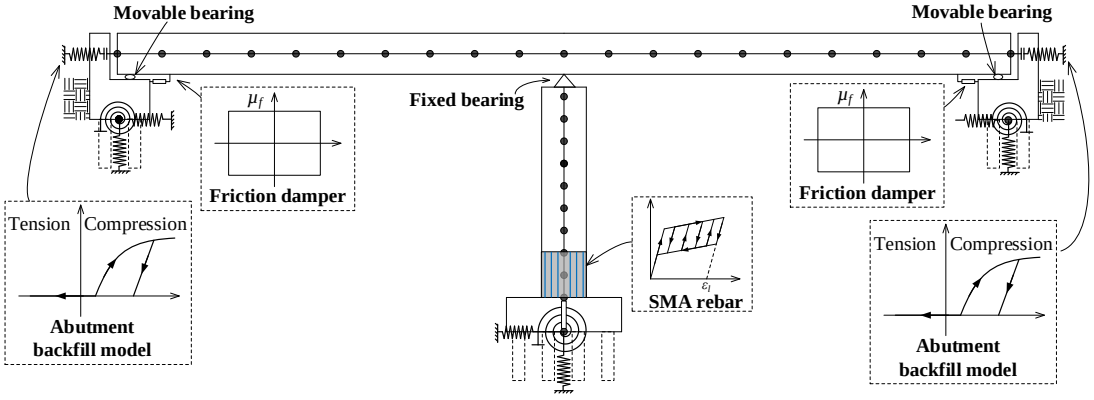

Fig. 1 Description of bridge models established in OpenSees

As the alternative strengthening measures, NiTi SMA reinforcing bars can be implemented at the plastic hinge region of the RC pier columns to replace the previous steel rebars. The austenite to martensite starting stress of the adopted SMA rebars is 401 MPa, which is similar to the yield stress of the steel rebars. This indicates that the equal-amount-replacement of steel rebars by SMA rebars can achieve the same design

lateral strength for the fixed pier. The other critical parameters of the SMAs can found in Xiang et al. (2020). The regions out of the plastic hinge still maintain the conventional steel reinforcement. Additionally, friction dampers are installed at the end abutments to restrain the superstructure displacements through frictional energy dissipation. These two measures are adopted either in individual or in combination to generate different bridge systems for analysis.

The bridge models are established in the FEM software framework OpenSees for nonlinear dynamic analyses, as shown in Fig. 1. Assuming the superstructure girders behave in elastic range under seismic loads, elastic beam-column elements are used to model the behaviour of the girders with the necessary properties including stiffness and mass specified. As the essential seismic resistant members of the bridge, the fixed pier is expected to undergo inelastic deformations, which will be modelled by using fiber-based nonlinear beam-column elements. The fibers are used to characterize the nonlinear behaviours of the unconfined and confined concrete, as well as the steel or SMA reinforcement. The Concrete01WithSITC material model in OpenSees is adopted to model the constitutive behaviour of the concrete, which can provide better estimates of residual deformations of RC columns (Lee and Billington 2010). The nonlinear behaviours of the steel rebars are modelled using the Steel02 material, which is the Giuffré-Menegotto-Pinto model with isotropic strain hardening. The behaviours of the SMA rebars are represented by the SelfCentering material, which as the material tag indicates, is able to simulate the typical flag-shaped or self-centering hysteretic responses. For friction dampers, an elastic-perfectly-plastic material by specifying a small yield displacement (e.g., 1mm) in OpenSees is adopted to approximately model the frictional sliding behaviour of the supplemental dampers, which can provide satisfactory response simulation (Xiang and Alam 2019). The effect of the abutment backfill is considered, and the Hyperbolic Gap material with recommended parameter values for dense sand is used for modelling (Wilson and Elgamal 2006). The flexibility of pile foundations is modelled by elastic spring elements, as shown in Fig. 1.

3. DESIGN OF INVESTIGATED BRIDGE SYSTEMS

3.1 Balanced design concept of SMA system

SMAs typically display flag-shaped hysteretic curves under cyclic loads, from which the capacities of full self-centering and some energy dissipation can be identified. The flag-shaped response curves can be approximately divided into two parts: a bilinear elastic curve and a bilinear elasto-plastic curve, which represent the self-centering and the energy dissipation of SMAs, respectively. The decomposition of the SMA flag-shaped models is shown in Fig. 2a, with the following equations required to be satisfied. The denotation of the symbols can be found in Fig. 2a.

$$f_{P1} - f_y = f_{T1} - f_{T2} \qquad f_{T2} = f_{ys} - f_{ye} \qquad f_y = f_{ys} + f_{ye} \tag{1}$$

To evaluate the relative force contributions between self-centering and energy dissipation of SMAs, a nondimensional index, λ, denoted as the ratio between the self-centering force and the energy dissipation-related force, is defined as follows:

$$\lambda = \frac{f_{ys}}{f_{ye}} \tag{2}$$

When λ is equal to 1.0, the balance between self-centering and energy dissipation can be achieved, whereas cases with λ lower and larger than 1.0 indicate the over-energy-dissipation and over-self-centering, respectively. It is obvious to find that the λ values of pure SMAs are generally larger than 1.0, for typical NiTi SMA , λ = 2.74-2.9 at the material stress-strain level (Xiang et al. 2020), which indicates that there is still room for the increase of energy dissipation for SMAs. As shown in Fig. 2a, it is possible to combine SMAs with conventional energy dissipation mechanisms like friction to further balance between the self-centering and energy dissipation capacities. In such cases, Eq. (2) can be rewritten as

$$\lambda = \frac{f_{ys}}{f_{ye} + f_s} \tag{3}$$

By adjusting the value of friction force, f_s, the evaluation index λ can varied approaching to 1.0. Alternatively, putting excessive friction would lead to λ values lower than 1.0.

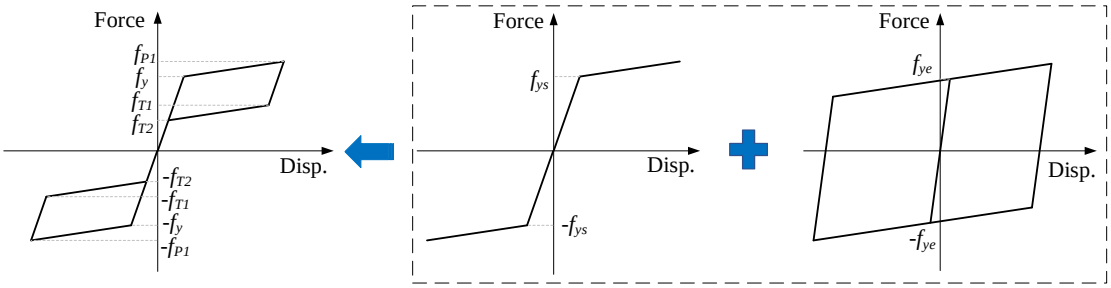

(a) Decomposition of SMA flag-shaped response curves

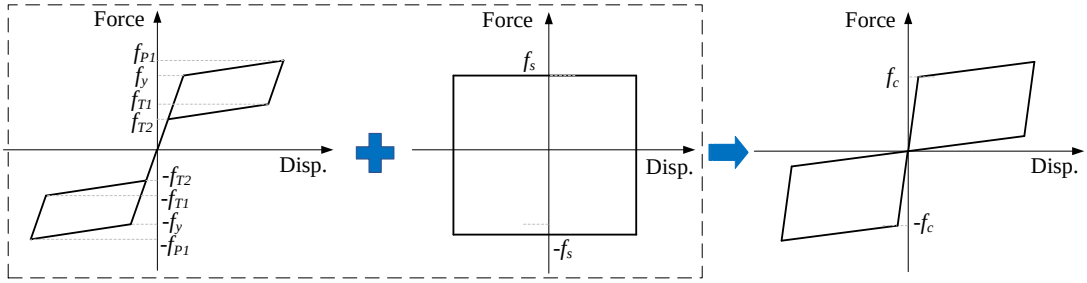

(b) Balanced combination of SMAs with friction dissipation

Fig. 2 Decomposition and combination of SMAs between self-centering and energy dissipation capacities

3.2 Design parameters for different bridge systems

In the current study, four longitudinal bridge systems are designed and analyzed, including the prototype one without SMAs or friction (Prototype), the one with pure SMA rebars (pure SMA, λ>1.0), the one with balanced SMA rebars and friction dampers (SMA+Friction I, λ=1.0), and the one with excessive friction (SMA+Friction II, λ<1.0). To conduct a fair comparison, the design of these four systems should follow the basic requirement that the design strength of the overall bridge systems should be almost the same, which can be evaluated through static pushover analysis. For simplicity, the design strength of the prototype system with only steel reinforcement is set as the benchmark for the other three systems. For the pure SMA system, such a design objective can be easily achieved by replacing the steel rebars with the same volume of SMA rebars at the plastic hinge regions. For the SMA+Friction systems, Eqs. (1)-(3) can be used to design the relative forces of the SMA-reinforced piers and the friction dampers to satisfy both the requirements of system design strength and λ values. Table 1 lists the obtained design parameters for the four longitudinal bridge systems. It can be seen from Table 1 that the strengthened bridge systems are designed to have the similar strength as the prototype for the fair comparison of relative seismic performance. For the pure SMA system, the estimated λ value is 3.31 when the reinforcement ratio is taken as 2.0%, indicating an over-self-centering design possible for further improvement. For this, friction dampers are added, as shown in the SMA-Friction I system, and λ is adjusted as 1.07 with the SMA reinforcement ratio of 1.25 % and the friction force designed as 600 kN. To design an over-energy-dissipation system for comparison, SMA-Friction I is also designed with the resultant reinforcement ratio of 0.67 % and the friction force of 1600 kN.

Table 1 Design parameters of different longitudinal bridge systems

Bridge system	Design strength (kN)	Reinforcement ratio (%)	Friction force (kN)	λ
Prototype	2892	2.0 (Steel)	0	N.A.
Pure SMA	2810	2.0 (SMA)	0	3.31
SMA+Friction I	2838	1.25 (SMA)	900	1.07
SMA+Friction II	2802	0.63 (SMA)	1600	0.44

Note: The friction force refers to the sum of all the friction dampers installed in the bridge.

4. PUSHOVER ANALYSIS OF BRIDGE SYSTEMS

In order to grasp the progressive force-displacement relationships of the considered bridge systems, static pushover analyses are conducted. The pushover force is taken as the sum of longitudinal reactions at the pier columns and abutments excluding the backfill reaction, whereas the girder displacement response is used as the pushover displacement. Fig. 3a-b shows the results of the monotonic and single loading-unloading pushover analyses, respectively. It can be seen from Fig. 3a that with the design parameters given in Table 1, the design yield strengths of the strengthened bridge systems (Pure SMA, SMA+Friction I, and SMA+Friction II) can reach close to the prototype strength. Regarding the ultimate lateral displacements, it is seen that using the

strengthened measures, the ultimate displacement capacity of the bridge system can be significantly increased. The SMA+Friction I has the largest ultimate displacement (0.875 m), followed by the Pure SMA (0.76 m), SMA+Friction II (0.693 m), compared with the Prototype system (0.468 m). In Fig. 3b, the single loading-unloading curves of the bridge systems are presented, with all the systems pushed to the same peak displacement (0.4 m). It can be seen from Fig. 3b that upon unloading, the pure SMA can achieve fully recentering behavior with the neglectable residual displacement of 0.006 m. Compared with the pure SMA system, the prototype and SMA+Friction II systems show large unloading residual displacements of 0.398 m and 0.292 m, respectively, accounting for 99.5% and 73.0% of the peak displacements, respectively. The residual displacement of the balanced SMA+Friction I system is found to be 18.8% of the peak displacement, reaching 0.075 m.

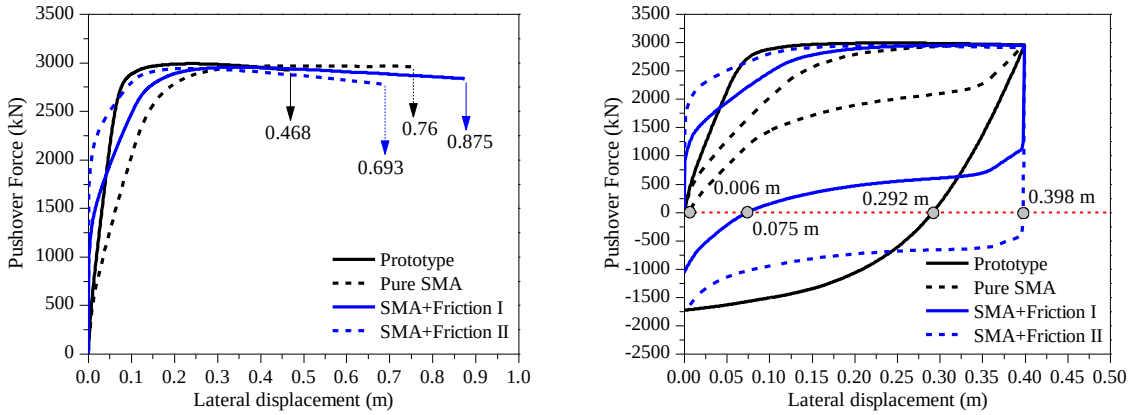

(a) Monotonic curve (b) Single loading-unloading curve

Fig. 3 Results of monotonic and single loading-unloading pushover analyses

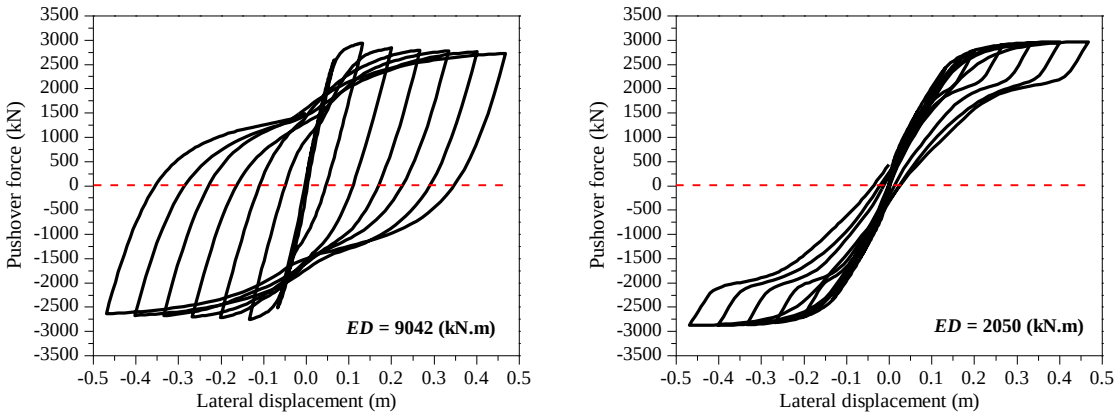

(a) Prototype (b) Pure SMA

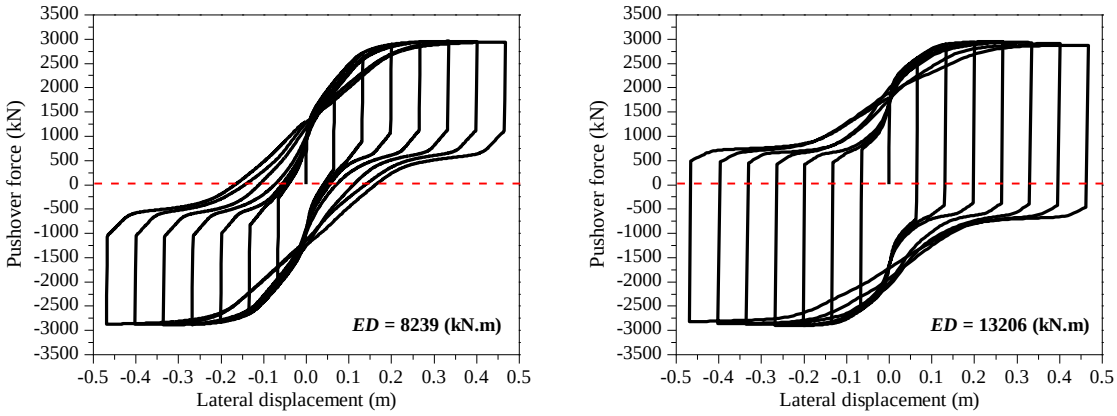

(c) SMA+Friction I (d) SMA+Friction II

Fig. 4 Results of cyclic pushover analyses

Fig. 4 shows the force-displacement hysteretic response curves of the bridge systems under cyclic loads. The cyclic loading patterns are set same for all the systems for the purpose of comparison. Compared with the Prototype curves showing the typical hysteresis of RC structures (shown in Fig. 4a), using SMAs will shrink the hysteretic curves to the flag-shaped ones, as depicted in Fig. 4b. The energy dissipation of the SMA system, as characterized by the areas of the enveloped hysteresis, is reduced yet the significant recentering behavior upon unloading can be achieved. When friction dampers are added to the SMA system, as shown in Figs. 4c and d, the hysteretic curves are expanded due to the energy dissipation contributions from the dampers. If the design force of the friction dampers are chosen appropriately, as indicated in the case of SMA+Friction I (Fig. 4c), the energy dissipation of the bridge system can be significantly improved without sacrificing much self-centering capacity. However, the over-implementation of the friction dampers may lose the self-centering behavior although the dissipated energy is exceptionally enhanced (shown in Fig. 4d). The dissipated energy summed up from the cyclic hysteresis is also given in Fig. 4, denoted as ED. The complete replacement of steel by SMA reinforcement will lead to the 77.3% reduction of ED, from 9042 kN.m to 2050 kN.m. Using the friction dampers with the balanced design, the value of ED can be well increased to 8239 kN.m, comparable to that of the prototype. The self-centering capacity, however, when comparing the hysteretic curves in Figs. 4a and c, can be remarkably obtained.

4. NONLINEAR DYNAMIC ANALYSIS OF BRIDGE SYSTEMS

4.1 Selected ground motions

In order to conduct the nonlinear time-history analysis, seven real earthquake ground motions are selected from the PEER Strong Ground Motion Database, as summarized in Table 2. The selected ground motions have distances to fault from 12.8 km to 26.2 km, with the original PGAs from 0.224 g to 0.568 g. Further, the ground motions are scaled appropriately to represent the design earthquake, and the scaled acceleration spectra are plotted in Fig. 5, from which it can be seen that they match well with the design spectrum. The seven scaled ground motions will be input in the bridge

models individually in the longitudinal direction of the bridge, and the individual responses are obtained and averaged for illustration.

Table 2 Summary of selected real earthquake ground motions

No.	Earthquake event	Year	Magnitude	Station	Distance to fault (km)	PGA (g)
1	Kobe	1995	6.9	Kakogawa	22.5	0.345
2	Kobe	1995	6.9	Abeno	24.9	0.224
3	Chi-Chi	1999	7.6	TCU045	26.0	0.361
4	Friuli, Italy	1976	5.2	Tolmezzo	26.2	0.351
5	Imperial Valley	1979	5.0	El Centro Array #2	18.8	0.315
6	Loma Prieta	1989	6.9	Gilroy Array #3	12.8	0.367
7	Northridge	1994	6.7	Castaic-ORR	20.7	0.568

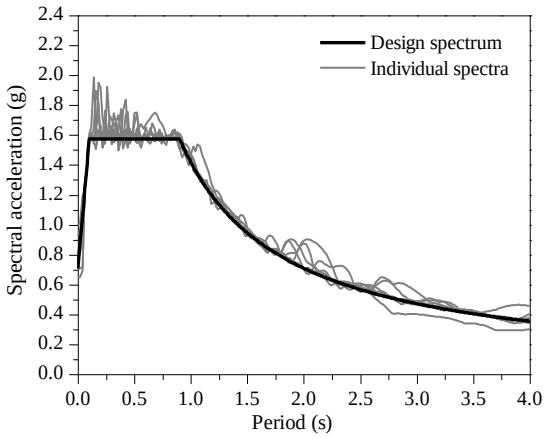

Fig. 5 Scaled acceleration spectra matched to design spectrum

4.2 Comparison of dynamic responses

For the considered bridge system that is a two-span continuous structure, three seismic responses are essential, which are the peak girder displacement (D_p), the residual girder displacement (D_r), and the energy dissipation (ED). For this, the demand-to-capacity ratio (DCR), the residual displacement ratio (RDR), and the energy dissipation ratio (EDR) are used to characterize these three responses, respectively, which are defined as

$$DCR = \frac{D_p}{D_c} \times 100\%, \qquad RDR = \frac{D_r}{D_p} \times 100\%, \qquad EDR = \frac{E_h}{E_s} \tag{4}$$

where D_c is the estimated ultimate displacement capacity of the bridge systems from the pushover analysis, as previously given in Fig. 3a. It is obvious to see that the values of DCR can provide effective evaluation for the failure, un-failure, and safety

redundancy of the bridge systems. Regarding the *RDR*, it is worth noting that a large peak displacement would generally result in a large residual displacement. Using *RDR* which is the ratio between residual displacement to peak displacement instead of D_r, the relative self-centering performance among different bridge systems can be assessed and compared more effectively since the effect of peak displacement is included. E_h and E_s are the hysteretic energy dissipated throughout the excitation and the elastic strain energy, respectively. The normalized *EDR* is expected to provide effective comparisons of relative energy dissipation capacities among different systems.

Figs. 6a-c show the comparisons of DCR, RDR, and EDR, respectively, for different bridge systems under design (DEQ) and 1.5 times of design earthquakes (1.5DEQ) averaged from the seven ground motions. It can be seen from Fig. 6a that the prototype bridge system has the largest *DCRs*, followed by the pure SMA, SMA+Friction I and II. The *DCRs* of SMA+Friction I and II systems are almost the same, lower than those of the pure SMA system. This indicates that with the similar design strength, the implementations of SMAs and friction dampers to replace conventional steel reinforcement can reduce the failure risk of the bridge systems. Regarding the *RDRs*, it can be seen from Fig. 6b that the prototype system has larger RDRs than the other three systems, which are 14% and 24%, respectively, for DEQ and 1.5DEQ. Although it is obvious to see that adding SMAs significantly reduces the values of RDR due to the unique self-centering capacity of SMAs, the benefits of SMAs can be overwhelmed with the excessive friction dampers. Taking the earthquake level of DEQ as an example, the SMA+Friction II shows the increased RDR of 8.5%, compared with the value of 1.3% for the Pure SMA system. With the balanced SMAs and friction design, as indicated in the system of SMA+Friction I, its RDR is found to be 2.5% at DEQ, much lower than that of SMA+Friction II. Regarding the energy dissipation capacity indicated by EDR, it can be seen from Fig. 6c that using pure SMAs to replace steel reinforcement will significantly reduce the energy dissipation of the bridge system. That is reason why the friction dampers are added to combine the SMAs. For instance, at 1.5 times of DEQ, the prototype system has the EDR value of 9.7, compared to the value of 4.5 for the Pure SMA. When the supplemental friction is added, as seen in SMA+Friction I and II, the values of EDR can be increased to 9.8 and 11.4, respectively.

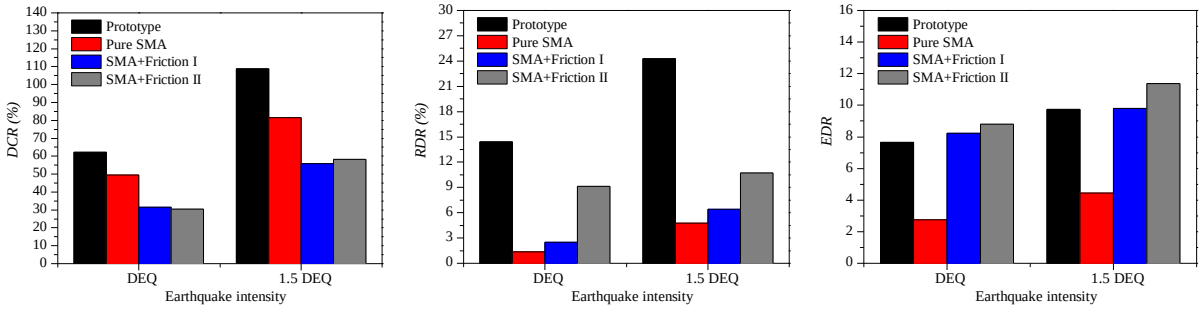

(a) DCR (b) RDR (c) EDR

Fig. 6 Comparison of seismic responses of different bridge systems

In order to provide a more detailed comparison of responses among different bridge systems, sample displacement histories and force-displacement hysteresis are plotted in Fig. 7, taking No. 4 earthquake (Friuli, Italy, 1976) as an example. It is seen from Fig. 7a that the Pure SMA shows larger absolute peak displacement than the other three systems, while the SMA+Friction II with the excessive energy dissipation has the smallest. For residual displacement responses, the prototype system is found to have the largest residual displacement of 0.175 m, followed by SMA+Friction II with 0.125 m, SMA+Friction I with 0.071 m, and Pure SMA with 0.039 m. It should be noted that although the SMA+Friction II system has the smallest peak displacement response, it leads to the second largest residual displacement among all the systems, which indicates that the over-use of energy dissipation to SMAs may considerably reduce the self-centering capacity of the bridge system. Figs. 7b and c plot the overall force-displacement hysteretic curves for different bridge systems, where it can be seen that in general, the shapes of the hysteresis look similar to those obtained from the pushover analyses. The relative performance of self-centering and energy dissipation for different systems can also be identified through the general shapes of the hysteretic curves.

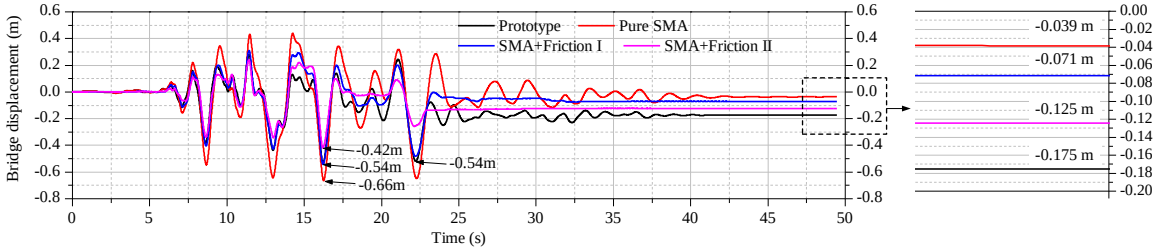

(a) Time-histories of bridge displacement

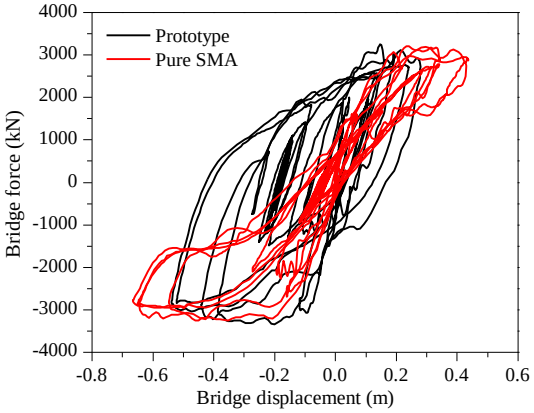

(b) Hysteresis of Prototype and Pure SMA

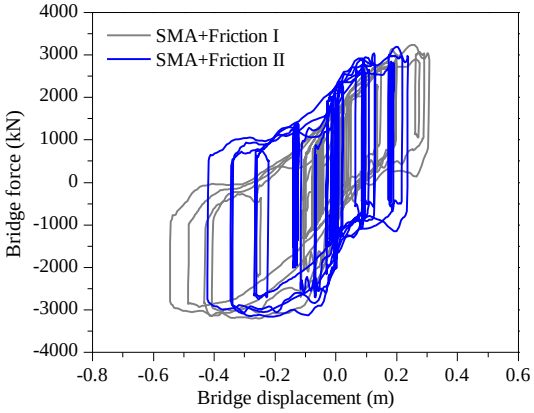

(c) Hysteresis of SMA+Friction I and II

Fig. 7 Sample displacement histories and cyclic hysteresis for different bridge systems (No.4 earthquake)

5. CONCLUSIONS

According to the balanced design concept between energy dissipation and self-centering capacities, this study proposes a novel longitudinal self-centering system for RC continuous bridges, composing of SMA reinforced piers and friction dampers at abutments. The relative amounts of SMAs and friction are appropriately designed for a balanced seismic performance of the bridge system. The study points to the following conclusions:

(1) The nondimensional index, λ, can be used to design the relative amounts between SMAs and friction for a balanced seismic design concept of self-centering and energy dissipation capacities.
(2) It can be seen from the pushover results that the energy dissipation capacity of the SMA system, as indicated by the hysteresis envelope areas, can be significantly enhanced by using the friction damping mechanism. By adjusting the relative design parameters of SMAs and friction dampers, a balanced design can be achieved that the overall energy dissipation of the bridge system is increased considerably without losing much self-centering capacity.
(3) The results of the nonlinear time-history analyses indicate that the balanced design of the bridge system (SMA+Friction I) can significantly reduce the peak displacement-capacity ratios compared with the pure SMA system, while maintaining a comparable effectiveness in mitigating the residual deformations of the bridge system under design and larger than design earthquakes. The over-use of friction, as indicated in SMA+Friction II, may reduce the self-centering capacity of the system by generating large residual deformations although the energy dissipation can be dramatically increased.

ACKNOWLEDGMENTS

The research described in this paper was financially supported by Japan Society for the Promotion of Science (JSPS) KAKENHI (Grant No. 20 K14811).

REFERENCES

Billah, A. M., and Alam, M. S. (2016), “Plastic hinge length of shape memory alloy (SMA) reinforced concrete bridge pier”, *Eng Struct*, **117**, 321-331.

Billah, A. M., and Alam, M. S. (2018), “Probabilistic seismic risk assessment of concrete bridge piers reinforced with different types of shape memory alloys”, *Eng Struct*, **162**, 97-108.

Chen, X., Xia, X., Zhang, X., and Gao, J. (2020), “Seismic performance and design of bridge piers with rocking isolation”, *Struct Eng Mech*, **73**(4), 447-454.

Japan Road Association (2002), “Specifications for highway bridges: Part Ⅴ seismic design”, Tokyo, Japan.

Kawashima, K., MacRae, G. A., Hoshikuma, J. I., and Nagaya, K. (1998), “Residual displacement response spectrum”, *J Struct Eng*, **124**(5), 523-530.

Lee, W. K., and Billington, S. L. (2010), “Modeling residual displacements of concrete bridge columns under earthquake loads using fiber elements”, *J Bridge Eng*, **15**(3), 240-249.

Li, J., Peng, T., and Xu, Y. (2008), “Damage investigation of girder bridges under the

Wenchuan earthquake and corresponding seismic design recommendations", *Earthq Eng Eng Vib*, **7**(4), 337-344.

Marriott, D., Pampanin, S., and Palermo, A. (2009), "Quasi-static and pseudo-dynamic testing of unbonded post-tensioned rocking bridge piers with external replaceable dissipaters", *Earthq Eng Struct D*, **38**(3), 331-354.

Shrestha, B., and Hao, H. (2016), "Parametric study of seismic performance of super-elastic shape memory alloy-reinforced bridge piers", *Struct Infrastruct E*, **12**(9), 1076-1089.

Wilson, P and Elgamal, A (2006), "Large scale measurement of lateral earth pressure on bridge abutment back-wall subjected to static and dynamic loading", *Proceedings of the New Zealand Workshop on Geotechnical Earthquake Engineering*, University of Canterbury, Christchurch, New Zealand: pp 307-315.

Xiang, N., Chen, X., and Alam, M. S. (2020), "Probabilistic seismic fragility and loss analysis of concrete bridge piers with superelastic shape memory alloy-steel coupled reinforcing bars", *Eng Struct*, **207**, 110229.

Xiang, N., and Alam, M. S. (2019), "Comparative seismic fragility assessment of an existing isolated continuous bridge retrofitted with different energy dissipation devices", *J Bridge Eng*, **24**(8), 04019070.

Yang, C., and Okumus, P. (2017), "Ultrahigh-performance concrete for posttensioned precast bridge piers for seismic resilience", *J Struct Eng*, **143**(12), 04017161.

Kawashima, K. (2012), "Damage of bridges due to the 2011 Great East Japan Earthquake", *Journal of Japan Association for Earthquake Engineering*, **12**(4), 4_319-4_338.

Akiyama, M., Takahashi, Y., Hata, Y., and Honda, R. (2016), "Lessons from the 2016 Kumamoto earthquake based on field investigations of damage to bridges", *International Journal of Earthquake and Impact Engineering*, **1**(3), 225-252.